Title

AAVR-Displaying Interfaces: Serotype-Independent Adeno-Associated Virus Capture and Local Delivery Systems

Authors

Kim, Seung-Hyun
Lee, Slgirim
Lee, Heehyung
et al.

Publication Date

2019-12-01

DOI

10.1016/j.omtn.2019.09.015

Peer reviewed

Molecular Therapy
Nucleic Acids
Original Article

AAVR-Displaying Interfaces: Serotype-Independent Adeno-Associated Virus Capture and Local Delivery Systems

Seung-Hyun Kim,[1,6] Slgirim Lee,[1,2,6] Heehyung Lee,[1] Mira Cho,[1] David V. Schaffer,[3,4,5] and Jae-Hyung Jang[1]

[1]Department of Chemical and Biomolecular Engineering, Yonsei University, Seoul 120-749, Korea; [2]Simpson Querrey Institute for BioNanotechnology, Northwestern University, Chicago, IL 60611, USA; [3]Department of Chemical and Biomolecular Engineering, University of California, Berkeley, Berkeley, CA 94720-3220, USA; [4]Department of Bioengineering, University of California, Berkeley, Berkeley, CA 94720-3220, USA; [5]Helen Wills Neuroscience Institute, University of California, Berkeley, Berkeley, CA 94720-3220, USA

Interfacing gene delivery vehicles with biomaterials has the potential to play a key role in diversifying gene transfer capabilities, including localized, patterned, and controlled delivery. However, strategies for modifying biomaterials to interact with delivery vectors must be redesigned whenever new delivery vehicles and applications are explored. We have developed a vector-independent biomaterial platform capable of interacting with various adeno-associated viral (AAV) serotypes. A water-soluble, cysteine-tagged, recombinant protein version of the recently discovered multi-AAV serotype receptor (AAVR), referred to as cys-AAVR, was conjugated to maleimide-displaying polycaprolactone (PCL) materials using click chemistry. The resulting cys-AAVR-PCL system bound to a broad range of therapeutically relevant AAV serotypes, thereby providing a platform capable of modulating the delivery of all AAV serotypes. Intramuscular injection of cys-AAVR-PCL microspheres with bound AAV vectors resulted in localized and sustained gene delivery as well as reduced spread to off-target organs compared to a vector solution. This cys-AAVR-PCL system is thus an effective approach for biomaterial-based AAV gene delivery for a broad range of therapeutic applications.

INTRODUCTION

Adeno-associated virus (AAV)-based gene delivery vectors have gained widespread attention due to their progressively stronger record of safety and efficacy in clinical trials,[1–3] including hemophilia B and A (using AAV8 and AAV5), spinal muscular atrophy (AAV9), and lipoprotein lipase deficiency (AAV1).[4–7] This record recently led to two US Food and Drug Administration approvals of gene therapies for the rare diseases Leber's congenital amaurosis and spinal muscular atrophy. However, numerous challenges remain in the field, including problems with delivery efficiency and controlled biodistribution. For example, even local injections of AAV into tissues such as muscle or CNS result in vector spread to distal tissues such as the liver,[8] which increases the risks of off-target side effects or immune responses. Additionally, a burst of gene expression following the injection of high doses of a vector risks toxicity,[3] and alleviating such concerns via multiple administrations of lower doses can increase medical costs and patients' inconvenience.[9] Thus, strategies to diversify the capabilities of AAV-mediated gene delivery systems (i.e., localized, sustained, and/or controlled delivery) may address these concerns and thereby further boost therapeutic efficacy.

Binding or adsorbing AAV vectors onto biomaterial surfaces and locally administrating the resulting "composites" to a target tissue or organ is an alternative strategy for overcoming limitations with direct virus injection.[10,11] For example, vector immobilization to a biomaterial can reduce systemic spread or leakage while increasing vector residence time in the target cellular microenvironment, thereby potentially restricting gene expression to the injected region.[12,13] Vector "loading" onto a biomaterial can be mediated by either non-specific adsorption[14–19] or specific affinity binding.[20,21] For example, we have bound vectors to the surfaces of materials modified with adhesives or charged moieties, even in a spatially dependent manner.[15] Similarly, we have inserted a hexa-histidine affinity tag onto AAV for immobilization onto nickel-presenting surfaces,[20] and, in other work, the insertion of an epitope onto the vector has enabled antibody-mediated incorporation into a material.[21] However, different therapeutic applications necessitate the use of different AAV variants or serotypes[2] (as evident from the range of AAVs used in promising trials to date: AAV1, AAV2, AAV5, AAV8, and AAV9[4–7]) such that strategies for biomaterial immobilization must be newly designed on demand to specifically incorporate the chosen AAV vector. Moreover, altering AAV capsids to mediate interactions with a biomaterial can alter their gene delivery properties, potentially negating the advantages of biomaterial-mediated delivery. For all these reasons, a versatile system that can interact

Received 28 August 2018; accepted 17 September 2019;
https://doi.org/10.1016/j.omtn.2019.09.015.

[6]These authors contributed equally to this work.

Correspondence: David V. Schaffer, Department of Chemical and Biomolecular Engineering, University of California, Berkeley, Berkeley, CA 94720-3220.
E-mail: schaffer@berkeley.edu
Correspondence: Jae-Hyung Jang, Department of Chemical and Biomolecular Engineering, Yonsei University, Seoul 120-749, Korea.
E-mail: j-jang@yonsei.ac.kr

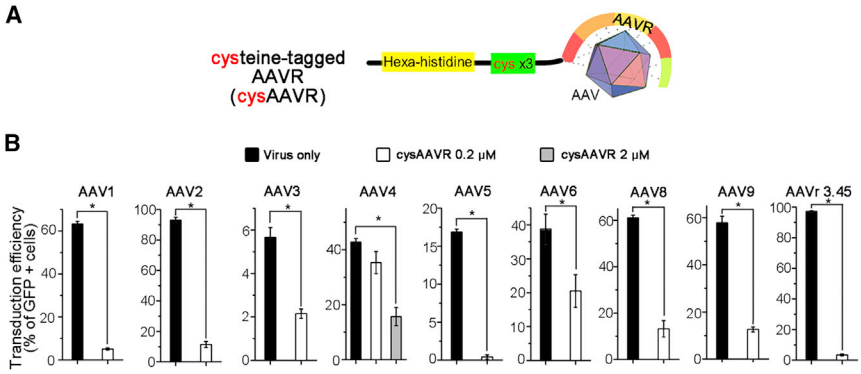

Figure 1. Production of cys-AAVR Proteins

(A) Peptide sequence of hexa-histidine/cysteine-tagged PKD1-5 domains (cys-AAVR), which possess a high affinity for AAV vectors. (B) Reduction of transduction efficiencies by AAV serotypes that interacted with free cys-AAVR proteins (0.2 or 2 μM). The genomic MOIs of each AAV vector were adjusted to obtain appreciable levels of transduction efficiencies in HEK293T cells (i.e., 1 X 10^5 for AAV1, -4, -5, -8, and -9 and 1 × 10^4 for AAV2, -3, -6, and -r3.45). *$p < 0.05$. Error bars represent SDs.

with the majority of AAV serotypes and newly emerging engineered variants would be impactful for biomaterial-mediated delivery.

Integrating components of glycans, which typically serve as initial receptors for AAV cell binding, into biomaterials offers a means of enabling AAV vector binding without altering viral capsids. For example, column-immobilized heparin and mucin—which present structures similar to those of heparan sulfate proteoglycan (HSPG) and sialic acid moieties, which serve as primary receptors for AAV2[22] and AAV5,[23] respectively—have been used for affinity binding of these serotypes.[24] However, because different AAV variants bind to alternate glycan receptors, different serotypes would necessitate different designs. Alternatively, a receptor that interacts with all of the AAV serotypes tested to date, denoted as the AAV receptor (AAVR), was recently identified.[25]

Here, we have developed an AAVR-functionalized biomaterial platform that can immobilize AAV vectors of various serotypes. Specifically, a water-soluble, cysteine-tagged recombinant version of the polycystic kidney disease (PKD) domains of AAVR protein, referred to as cys-AAVR, was linked by click chemistry to polycaprolactone (PCL) surfaces. The resulting "serotype-independent" cys-AAVR-PCL system demonstrated the versatile capacity to bind multiple AAV serotypes as well as an engineered AAV variant. Furthermore, the intramuscular injection of AAV-loaded biomaterials resulted in highly localized gene expression over extended periods and considerably less spread to off-targets tissues, such as liver and heart, compared to injection of a vector solution. Finally, specific interactions of the cys-AAVR-PCL system with AAV vectors enabled spatially patterned gene expression *in vivo*, corresponding to the structural morphology of implanted PCL material. By successfully integrating AAVR protein into biomaterials for the first time, this study offers new options for controlled AAV gene delivery.

RESULTS

Production of cys-AAVR Capable of Simultaneously Interacting with Multiple AAV Serotypes

A water-soluble, cysteine-tagged version of the AAVR ectodomain (cys-AAVR) containing the AAV-binding region[25] was designed for conjugation to the surface of polyester-based biodegradable/biocompatible PCL materials, which were formulated as either microspheres or electrospun fibrous matrices, to create a system for immobilizing AAV (cys-AAVR-PCL), as schematically shown in Figure 1A. The cys-AAVR was engineered with a hexa-histidine and three cysteine residues at the N terminus of the PKD1 domain to facilitate cys-AAVR protein purification and act as functional groups for biomaterial conjugation, respectively (Figure 1A). Rather than conjugating via lysine amino groups along the protein's native sequence, which can in general interfere with protein function, terminal cysteine thiols were selected as functional linkers.[26] The resulting histidine/cysteine-tagged AAVR protein was successfully expressed and purified from *E. coli*, resulting in the predicted 55 kDa molecular weight protein product (Figure S1).

The functionality of the cys-AAVR protein was assessed by testing its interactions with multiple AAV serotypes and an engineered variant: AAV1, -2, -3, -4, -5, -6, -8, and -9 and AAVr3.45 (a vector that was engineered for high efficiency transduction of neural stem cells and exhibits strong therapeutic potential[27–31]). Specifically, soluble cys-AAVR protein was mixed with each vector (packaged with cDNA encoding GFP), and the resulting solution was added to a cell culture. The transduction by all the AAV/cys-AAVR mixtures was significantly reduced compared to free, naive AAV vector (i.e., only virus) (Figure 1B), presumably due to the competitive inhibition of the binding of AAV to the cell surface AAVR.[25] As observed in previous studies, which reported that AAV4's infectious pathway does not involve AAVR-mediated internalization,[32] an exception was that the inhibition of AAV4 infection required a significantly higher concentration of cys-AAVR (2.0 rather than 0.2 μM; $p < 0.05$), and the inhibition was not always consistent. Therefore, we focused on serotypes other than AAV4 for all subsequent analysis.

Conjugation of cys-AAVR onto PCL Systems

cys-AAVR was conjugated to the surface of PCL via thiol-maleimide click chemistry. Two PCL material formats, microspheres (average diameter = 22.0 ± 9.3 μm) and fibrous structures (average fiber diameter = 0.63 ± 0.23 μm), were formulated by water-oil emulsion and an electrospinning process, respectively, prior to their surface modification (Figure 2A). Microsphere formulations have been

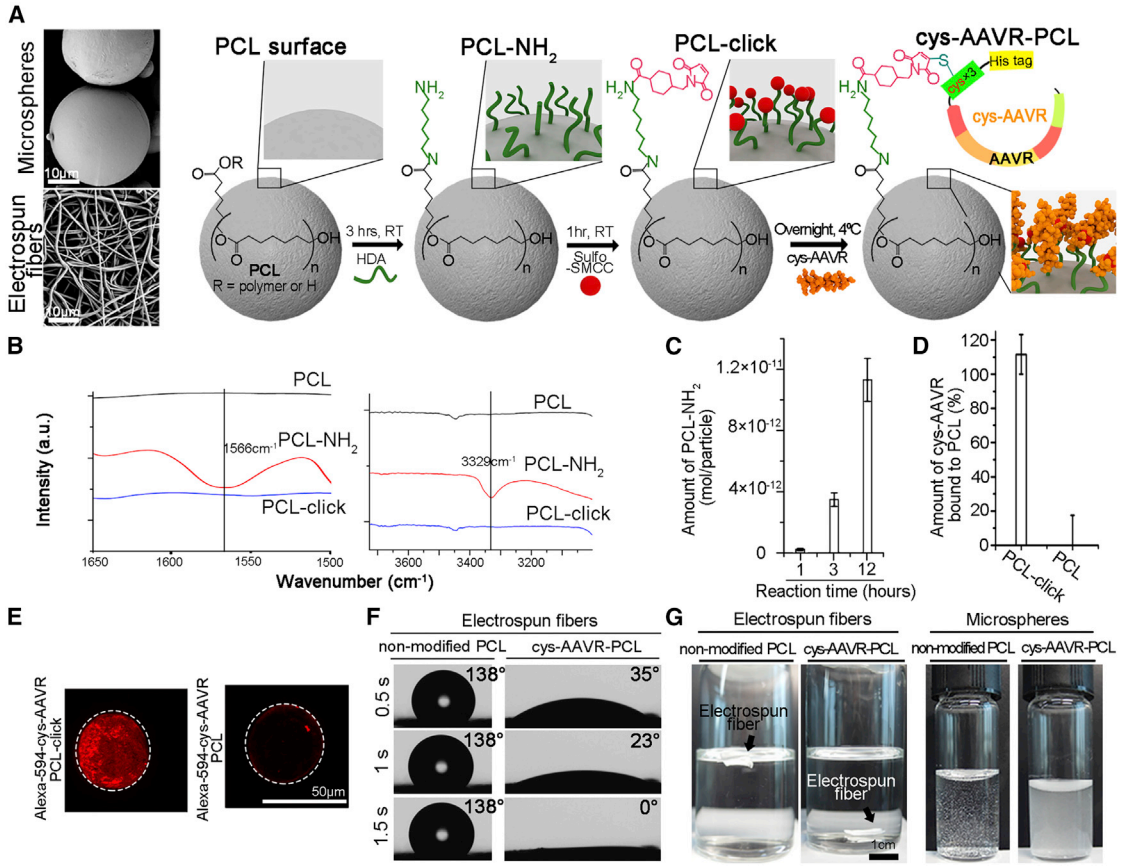

Figure 2. Preparation and Characterization of cys-AAVR-PCL Surfaces

(A) Reaction scheme to generate PCL-NH_2, PCL-click, and cys-AAVR-PCL microspheres. The SEM images in the top panel demonstrate the representative morphologies of PCL microspheres (top) and electrospun fibrous matrices (bottom). The ester bonds within the repeated units of PCL chains reacted with 1,6-hexanediamine (HDA) to generate amide bonds, consequently displaying primary amines on the PCL templates (PCL-NH_2). The resulting templates were treated with sulfo-SMCC to attach maleimide groups (PCL-click), which can, in turn, covalently react with the sulfhydryl groups on the cysteine chains of cys-AAVR. (B) FT-IR analysis of aminolyzed PCL (PCL-NH_2) and maleimide-displaying PCL (PCL-click) microspheres. (C) Quantity of exposed amines on PCL-NH_2 microspheres, which was measured by ninhydrin assay. (D) Quantification of cys-AAVR proteins that were conjugated to PCL-click microspheres. The quantity of cys-AAVR in the solution was measured using a BCA assay kit, and the percentage indicates the fraction of cys-AAVR that bound to the PCL-click microspheres relative to its initial amount. Error bars in (C) and (D) represent SDs. (E) Visualization of Alexa 594-tagged cys-AAVR proteins on PCL-click microspheres. The white dotted line illustrates the contour of a PCL microsphere. (F) Water contact angles on cys-AAVR-PCL or non-modified PCL electrospun fibrous matrices at 0.5, 1, and 1.5 s. (G) Different behaviors of cys-AAVR-displaying PCL electrospun fibrous matrix (left) and microspheres (right) in aqueous solution compared to those of non-modified naive PCL systems.

widely used as injectable carriers for surface-bound therapeutic agents (e.g., cells, gene vectors, and drugs) at defined locations.[33–35] In addition, electrospun materials—generated in an electrospinner via the application of an electrostatic force to a polymer solution to generate nano-/micro-scaled polymeric threads of dimensions that mimic the fibrous morphologies of extracellular matrices (ECMs)—can serve as physical supports for cells in gene therapy and tissue engineering applications.[36–38]

As schematically illustrated in Figure 2A, maleimide groups were displayed from the surfaces of both the PCL formats to covalently react with the sulfhydryl groups on the cysteine chains of cys-AAVR. First, the PCL surfaces were prepared via 1,6-hexanediamine (HDA)-mediated amination, resulting in absorption peaks for primary amines at 3,329 and 1,566 cm^{-1} (Figure 2B) that increased with the reaction time to a plateau of approximately 12.0 pmol of amines per PCL microsphere (Figure 2C). The amines were subsequently reacted with sulfosuccinimidyl-4-(N-maleimidomethyl) cyclohexane-1-carboxylate (sulfo-SMCC) to yield maleimides. Upon adding the resulting maleimide-activated PCL microspheres (i.e., PCL-click) to a cys-AAVR solution, nearly all of the free cys-AAVR was successfully captured onto the PCL surfaces, whereas, in contrast, the majority of cys-AAVR remained in solution when non-functionalized PCL microspheres were added (Figure 2D). Alexa-594-labeled cys-AAVR was used to visualize its immobilization, and abundant AAVR was observed on the PCL-click microsphere surface

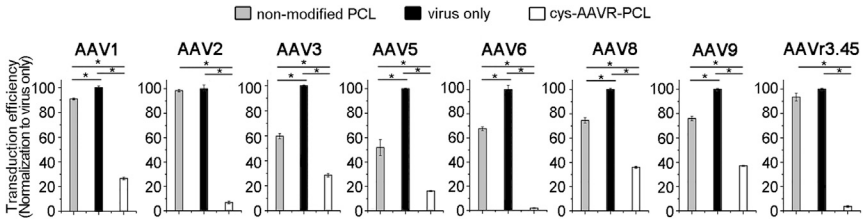

Figure 3. Capacity of cys-AAVR-PCL Microspheres to Capture Various AAV Serotypes

Various AAVs were incubated with cys-AAVR-PCL; moreover, naive viral supernatant (black bars), supernatants depleted by non-modified PCL microspheres (gray), or supernatants depleted with cys-AAVR-PCL (white) were incubated with HEK293T cells. Incubation with the cys-AAVR-functionalized microspheres uniformly depleted the infectious AAV from the lysates. The volume of cell lysates containing each AAV serotype was adjusted to obtain the highest transduction efficiencies for each AAV-GFP vector, and the same volume was utilized for interacting with the non-modified or cys-AAVR-PCL microspheres. High viral quantities (i.e., MOI of 1×10^5) were used to interact with each PCL microsphere set. Transduction efficiencies obtained by non-bound AAV vectors were normalized to those by virus only. *$p < 0.05$. Error bars represent SDs.

in contrast to the low fluorescence on the non-modified PCL microspheres (Figure 2E).

The cys-AAVR immobilization significantly altered the properties of the PCL-click surfaces, as assessed using electrospun fibrous surfaces, which are reasonably suited for water contact angle analysis of surface hydrophobicity/hydrophilicity. Water droplets promptly adhered to the cys-AAVR-PCL electrospun fibrous matrices, indicating the hydrophilic nature of the protein-modified surface: 35° at 0.5 s, 23° at 1 s, and 0° at 1.5 s. In contrast, high water-contact angles (138°) were consistently maintained on the non-modified PCL matrices (Figure 2F). As an alternate indicator, cys-AAVR-PCL electrospun fibers settled immediately to the bottom of the aqueous solutions, whereas the non-modified hydrophobic PCL matrices floated on the water surface (Figure 2G). Finally, cys-AAVR-PCL microspheres could be homogeneously dispersed in water for extended times, whereas an apparent phase separation was observed when non-modified PCL microspheres were present in the aqueous solutions (Figure 2G). In addition to indicating the occurrence of cys-AAVR immobilization, this transition of PCL into a hydrophilic surface is important for facilitating interactions with the AAV vectors suspended in the aqueous solution.

Viral Binding onto cys-AAVR-PCL Systems

The capacity of the cys-AAVR system to specifically capture AAV vectors was initially examined by comparing AAV9 binding to the surfaces of PCL microspheres for different modes (Figure S2): (1) different binding mechanisms (i.e., non-specific adsorption versus specific interaction), (2) different viral purity (purified vectors versus vectors in crude lysates), and (3) different affinity to cys-AAVR in different states (vector binding onto adhered cys-AAVR versus free cys-AAVR). Approximately 2-fold increases in specific interactions of AAV9 on the cys-AAVR-PCL microspheres occurred compared to non-specific adsorption on the non-modified PCL microspheres (Figure S2A). In addition, interactions of the cys-AAVR with AAV vectors were enhanced when viral vectors were previously purified rather than in crude lysates (Figure S2B). Finally, even in the presence of free cys-AAVR proteins, the cys-AAVR-PCL microspheres demonstrated a significantly improved ability to capture AAV compared to the non-modified PCL microspheres (Figure S2C). These results confirm specific interactions of cys-AAVR displayed on the PCL microspheres with AAV vectors.

We tested the capacity of cys-AAVR-PCL microspheres to capture various AAV serotypes, including AAV1, -2, -3, -5, -6, -8, and -9 and AAVr3.45, by evaluating the cellular transduction of non-bound AAV vectors (i.e., free vectors); robust interactions of AAVR with AAV vectors would reduce free viral vectors and result in decreases of cellular transduction by vectors in supernatant. Ten milligrams of cys-AAVR-PCL or non-modified PCL microspheres were added to HEK293T producer cell lysates containing each vector, followed by a 1-h incubation. The viral binding to cys-AAVR PCL microspheres was assessed in parallel as a control. Numerous proteins in cell lysates, including viral vectors, can be non-specifically adsorbed onto hydrophobic non-modified surfaces;[37] therefore, both PCL microsphere sets were pre-coated overnight with a surfactant (i.e., 0.01% [v/v] Tween 20) prior to the viral binding. The supernatants were then aspirated and transferred to fresh HEK293T cell cultures, such that the non-bound AAV could infect HEK293T cells. Regardless of the AAV serotype, substantial reductions in the percentage of GFP-expressing cells, ranging from 2.7- to 27-fold, were observed for the supernatants from cys-AAVR-PCL compared to those in the control non-modified microspheres (Figure 3). For example, incubation with AAV2 and AAVr3.45 vector stocks resulted in GFP expression in 91% and 98%, respectively, of 293T cells, whereas supernatants following the incubation of an identical dosage of vectors with cys-AAVR-PCL microspheres resulted in 6.3% or 3.7% GFP-positive cells. In the case of AAV9, a 2.7-fold decrease in the transduction was observed after the viral depletion with the cys-AAVR-PCL microspheres compared to the transduction with an equivalent dosage of vector stock. Binding efficiencies to the cys-AAVR-PCL microspheres were reproducibly significantly higher than that of the non-modified PCL microspheres ($p < 0.05$), demonstrating the specific interactions of the AAVR adhered to PCL microspheres with AAV vectors regardless of their serotypes.

cys-AAVR-PCL Systems for Localized and Sustained AAV Delivery

The capacity of cys-AAVR-PCL to function as a gene delivery carrier for *in vitro* transduction was initially evaluated using an electrospun

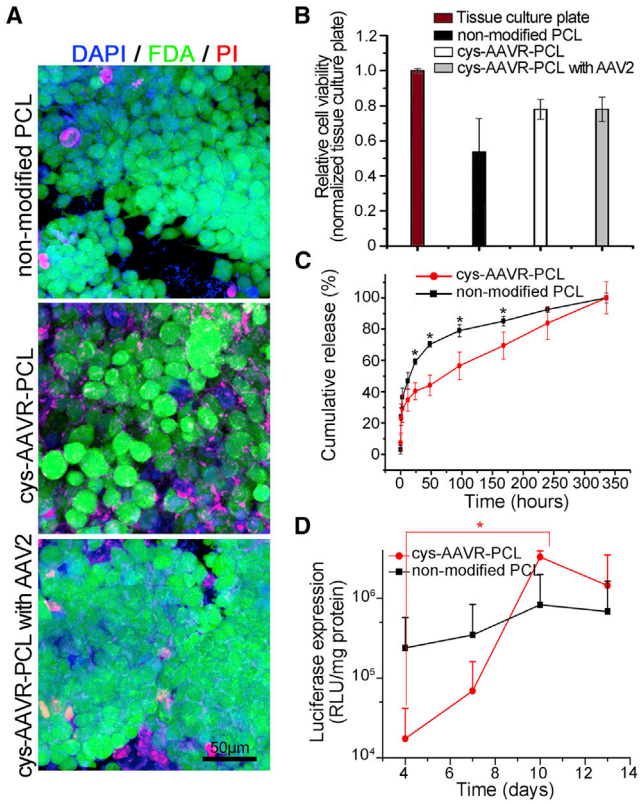

Figure 4. *In Vitro* Release Kinetics and Cellular Transduction on cys-AAVR-PCL Fibrous Matrices

(A) Fluorescence images of viable (fluorescein diacetate [FDA], green) and dead (propidium iodide [PI], red) HEK293T cells that were grown on cys-AAVR-PCL matrices with or without loaded AAV2 vector. The nuclei of the cells were counterstained with DAPI (blue). (B) Cellular proliferation (HEK293T cells) was measured by a colorimetric assay (cell-counting kit-8 [CCK-8]). (C) Cumulative release profiles of AAV2 vectors from cys-AAVR-PCL or non-modified PCL electrospun matrices. The fluorescence intensities of Alexa 594-tagged AAV vectors were measured at designated time points, and the cumulative releases were expressed as the ratio of the fluorescence intensities measured at each time point to those at the last time point (i.e., 336 h). (D) Time-dependent profiles (RLU/mg protein) of *in vitro* cellular transduction by AAV2 vectors that were immobilized onto cys-AAVR-PCL or non-modified PCL electrospun fibrous matrices. Error bars represent SDs.

fibrous formulation, rather than microspheres, due to the convenience of growing cells on their relatively flat surfaces. To analyze *in vitro* cellular transduction, AAV2 vector encoding luciferase (AAV2-luc) was adhered to a cys-AAVR-PCL fibrous matrix by gently agitating for 1 h followed by rinsing with PBS, and the resulting mixture was seeded with HEK293T cells. Cellular transduction was then monitored by quantifying luciferase expression. As controls, AAV2-luc vectors in suspension (1×10^9 viral genomes [vg]) were dropped and marginally air-dried on the non-modified PCL matrices without washing to conserve the initial viral quantities (i.e., 1×10^9 vg). To our knowledge, there is no method to examine cellular transduction profiles with identical viral quantities on each surface due to their different properties (non-modified PCL versus cys-AAVR-PCL matrices). Instead, time-dependent, characteristic delivery modes from each surface (e.g., rapid versus gradual increases), rather than a comparison of the delivery efficiencies of each system, were assessed.

Prior to analyzing the *in vitro* transduction, the biocompatibility of the cys-AAVR-PCL matrices or cys-AAVR-PCL with AAV2 was verified by the presence of high densities of live cells on their surfaces (Figure 4A). Cellular proliferation on the cys-AAVR-PCL matrices or cys-AAVR-PCL with AAV2 was not significantly different from that on tissue culture plates (Figure 4B). Next, the release kinetics of AAV vectors from the cys-AAVR-PCL systems were examined by tagging the AAV vectors with Alexa Fluor 594 followed by quantifying the time-dependent fluorescence intensities of the desorbed vector. Specific interactions of cys-AAVR with AAV vectors apparently reduced the initial burst release of vector and slowed subsequent release from the AAVR-PCL systems (i.e., electrospun matrices or microspheres) compared to that from the non-modified PCL (Figures 4C and S3). Furthermore, the *in vitro* cellular transduction profiles on each matrix correlated with the delivery trends observed in the release kinetics. That is, luciferase expression levels on the non-modified PCL fibrous matrices showed a faster onset of expression (<4 days) than that on the cys-AAVR-PCL matrices (Figure 4D). However, the specific loading of AAV onto the cys-AAVR-PCL matrices resulted in an apparent progressive viral release, indicated by gradually increasing luciferase expression,[20] and the levels of luciferase expression at 10 days post-transduction were significantly higher than those at 4 days post-transduction (Figure 4D). These results indicate that the cys-AAVR-PCL system can serve as a serotype-independent tool to modulate AAV delivery in a sustained manner compared to the non-modified systems.

Next, the potential for localized *in vivo* gene delivery was evaluated, and AAV9 was selected due to its muscle infectivity.[3,39] As schematically illustrated in Figure 5A, 10 mg of cys-AAVR-PCL microspheres or control non-modified PCL microspheres were added to AAV9-luc (5×10^{10} vg in 30 μL, previously purified via density ultracentrifugation). After gentle mixing, the whole suspension (30 μL) containing the same quantity (5×10^{10} vg) as the virus suspension was immediately injected into the mouse hind limb muscle (n = 6) without further treatment, such as removal of non-specifically bound vector with surfactant or removal of non-bound vector. In parallel, a purified AAV9 vector solution (30 μL; without interacting with PCL microspheres) was injected at an identical vector dosage (5×10^{10} vg). The AAV9-luc solution resulted in widespread luciferase expression, both in the hind limb as well as in the liver and heart (top panels of Figure 5B, shown with arrows), at levels maintained for the course of this study (Figure 5C). The injection of AAV9 mixed with non-modified PCL microspheres resulted in a marginal increase in the spread area of gene expression (i.e., region of interest [ROI] values drawn along the minimum luminescence signals) relative to those obtained by AAV9 delivery from cys-AAVR-PCL microspheres (Table S1) (middle and bottom panels of Figure 5B). This increase of the spread area, however, was not statistically significant at any time point

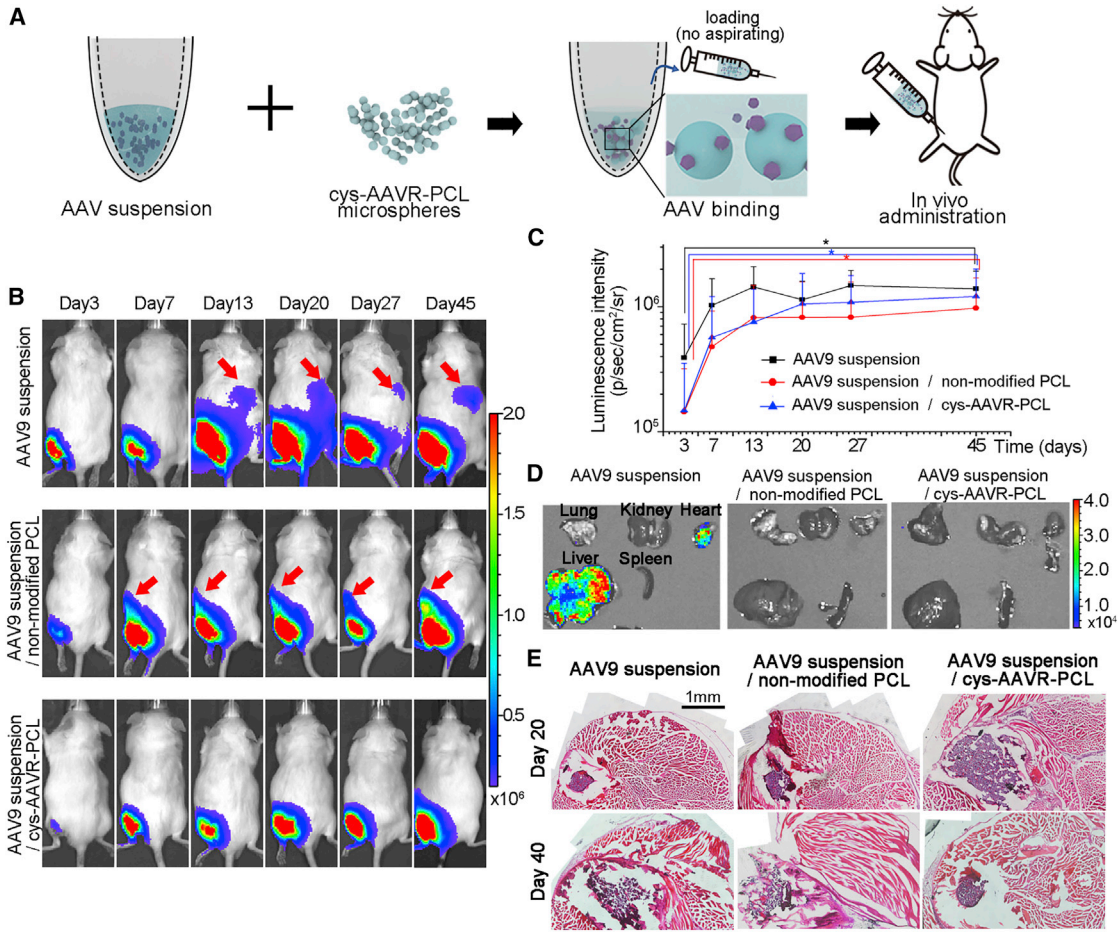

Figure 5. Localized Gene Delivery by AAV9 Loaded onto cys-AAVR-PCL Microspheres

(A) Schemes depicting the delivery system. cys-AAVR-PCL microspheres (10 mg) were dispersed in each viral sample (total of 5×10^{10} vg; iodixanol purified), and the resulting suspensions were intramuscularly injected into the mouse hind limb. Note that the non-modified PCL microspheres were pre-treated with Tween-20 to reduce the non-specific binding of AAV9 to the surfaces. Without rinsing and centrifugation, the suspensions containing virus and microspheres were injected immediately after each microsphere set was added to the suspension. (B) *In vivo* bioluminescence images of luciferase light signals emitted from transduced cells upon intramuscular injections of three groups: (1) only AAV9 solution (top, n = 6), (2) AAV9 solution with non-modified PCL microspheres (middle, n = 6), and (3) AAV9 solution with cys-AAVR-PCL microspheres (bottom, n = 6). (C) Time-dependent bioluminescence intensities (p/s/cm^2/sr) at 3, 7, 13, 20, 27, and 45 days. Error bars represent SDs. (D) Light signals from several representative organs (liver, spleen, heart, kidney, and lung). (E) H&E staining of muscle tissue isolated at 20 and 40 days post-injections. Multiple H&E-stained images were assembled to represent the whole tissue sections.

(Table S1). Finally, AAV9 immobilized to cys-AAVR-PCL microspheres, whose initial release rates (<4 days) were significantly slower than those from the non-modified PCL microspheres (Figure S3), which resulted in gradual increases in the light signals as well as strong light emission directly over the injection sites (bottom panels of Figure 5B). While the slow release from the cys-AAVR-PCL microspheres resulted in significantly lower gene expression at 7 days than that of the AAV9 solution, stable, localized gene expression was observed at the injection site for extended time periods at levels comparable to animals administered with soluble AAV or AAV with non-modified PCL microspheres (Figure 5C). These observations establish that the cys-AAVR-PCL materials can be utilized to mediate localized and sustained gene delivery at defined sites.

At 20 days post-injection, several organs, including the heart, liver, spleen, lung, and kidney, were harvested, and the luciferase signals from each organ were examined to further characterize off-target gene delivery. For animals injected with vector solution, high luciferase expression was observed in the liver and heart; however, in contrast, no signal was detected from any organ when AAV9 was administered in complex with cys-AAVR-PCL microspheres (Figure 5D). Similarly, in the absence of a step such as surfactant rinsing to remove non-specifically bound vector, animals treated with non-modified PCL microspheres also showed no expression in the liver or heart. Off-target gene delivery was examined by quantifying the levels of luminescence emitted from individual organs (Figure S4), and significantly

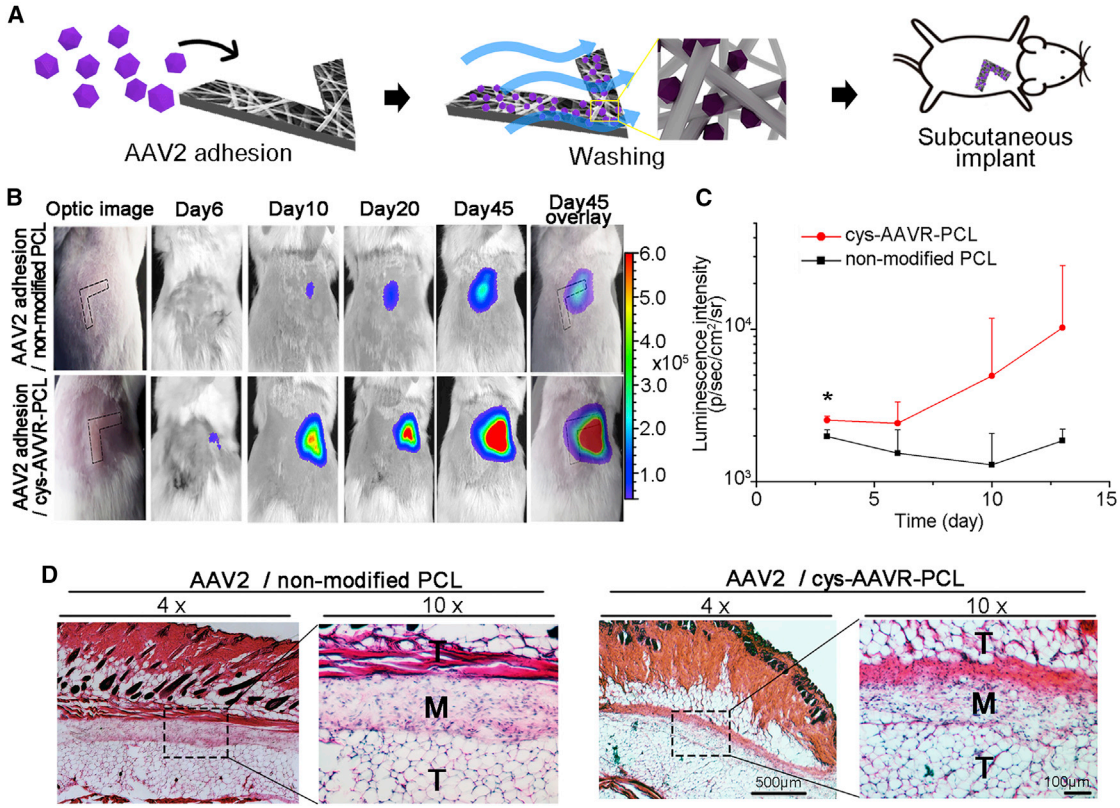

Figure 6. Spatially Patterned Gene Delivery by AAV Loaded onto cys-AAVR-PCL Matrices

(A) Schemes depicting the delivery system. AAV2-luc vectors (3×10^{10} vg) were adsorbed onto the cys-AAVR-PCL electrospun matrices with a spatial pattern (i.e., V pattern), which were subcutaneously implanted onto the back of mice. Non-modified PCL matrices were pre-treated with Tween-20 to reduce AAV2 non-specific binding to the surfaces. (B) *In vivo* bioluminescence images of luciferase light signals over the implanted matrices with spatial patterns: AAV2 with non-modified PCL matrix (top, n = 6) and AAV2 with cys-AAVR-PCL matrix (bottom, n = 6). The dotted line indicates the location of implanted matrices. (C) Bioluminescence intensities (p/sec/cm^2/sr) at designated time points (i.e., 3, 7, 10, and 13 days). The asterisk (*) indicates significant differences at identical time points. Error bars represent SDs. (D) H&E staining of tissue isolated at 45 days post-implantation. The letters "T" and "M" indicate surrounding tissues and matrices, respectively. The dotted regions correspond to the regions shown with high magnification.

enhanced luminescence (relative light units [RLU]/mg protein) compared to the level observed in negative controls (i.e., organs of non-infected animals) was detected in the muscle, heart, and liver of animals infected by vectors in solution. In contrast, the levels observed for AAV9/cys-AAVR-PCL from the majority of organs except for the injected muscle were similar to the ones for negative controls.

Mild immune infiltration was observed around the cys-AAVR-PCL microspheres or non-modified PCL microspheres in tissue sections obtained 20 days post-injection (Figure 5E). The majority of inflammatory cells regressed at later stages (40 days post-injection; Figure 5E), consistent with our observation that tumor necrosis factor-alpha (TNF-α) levels in plasma 45 days post-injection persisted at a basal level (Figure S5). Additionally, body weights of all animals showed no significant differences (Figure S6), further demonstrating the biocompatibility of the cys-AAVR-PCL-mediated AAV delivery.

Finally, the capacity of cys-AAVR-PCL systems to mediate another localized gene delivery mode (spatially patterned gene delivery) was investigated by subcutaneously implanting the composite of AAV2-luc/cys-AAVR-PCL electrospun matrices (or AAV2-luc/non-modified PCL matrices; n = 6) whose structural exteriors were confined into a specific shape (i.e., V pattern). As shown in Figure 6A, electrospun matrices (cys-AAVR-PCL or non-modified PCL) with a V pattern were manually formulated, and AAV2-luc vectors were immobilized on each surfactant-treated electrospun matrix. The resulting composites, which were vigorously rinsed with PBS prior to implantation to remove weakly-bound vector, were subcutaneously implanted into the back of mice, and the ability of cys-AAVR-PCL to mediate defined patterns of vector transduction corresponding to the shape of the original implanted matrices (i.e., V shape) was examined. Luciferase signals with spatial patterns gradually appeared as time elapsed, whereas the non-modified PCL matrices containing non-specifically bound AAV2-luc with low quantities (possibly due to surfactant rinsing) induced low levels of light signals without

confined patterns (Figure 6B). Importantly, as consistently observed in the intramuscular injections (Figure 5), apparent levels of light emission from the cys-AAVR-PCL electrospun matrices were detected progressively (>6 days post-transplantation) (Figures 6B and 6C), resulting in levels substantially higher than for non-modified PCL. For either of the delivery sets, no significant recruitment of inflammatory cells was observed around the implanted matrices (Figure 6D), further verifying the biocompatible properties of the electrospun cys-AAVR-PCL matrices releasing AAV vectors. In sum, the biomaterial gene delivery of an affinity-immobilized vector offers a broad and facile strategy for localized and sustained gene delivery.

DISCUSSION

The AAV-binding domain of the multi-AAVR was successfully conjugated to the biodegradable and biocompatible PCL materials (i.e., cys-AAVR-PCL), thereby allowing them to physically interface with AAV vectors, nearly regardless of serotype. This universal feature of the cys-AAVR-PCL clearly distinguishes it from other recent biomaterial-mediated gene delivery constructs by us and others, which are complicated by the need to design new biomaterial immobilization strategies for each serotype. The versatile AAVR-PCL composite reported here simultaneously addressees two challenges associated with AAV-mediated gene delivery: (1) serotype-independent AAV capture/binding with a single system and (2) localized/sustained delivery of AAV vector. No further decoration or modification of the biomaterials is required except for AAVR conjugation. Additionally, almost all naturally occurring AAV serotypes can be immobilized onto the AAVR system without chemical or genetic modifications, thereby conserving their inherent infectious properties. Moreover, there are no limitations in the biomaterial structures to functionalize their surfaces since the AAVR conjugation can be conducted once their exteriors are completely constructed via desired processes. Thus, the AAV serotype-independent platform system using AAVR can be employed for a broad range of AAV applications, from gene therapy and regenerative medicine to fundamental biological studies.

The building block material (e.g., PCL in this study) can be substituted, in principle, with any material with functional groups (e.g., dextran and Sepharose) capable of specifically reacting with thiols on the cys-AAVR (e.g., maleimide with thiols). Thus, the cys-AAVR-PCL system can be straightforwardly translated into any biocompatible material depending on a given gene therapy or tissue engineering application. It is also likely on this or other materials that vector capture and release can be modulated by adjusting the systems' spatial geometry or AAVR quantities/distribution on the surfaces. Furthermore, each AAV serotype differentially interacts with PKD domains 1–5;[40] thus, it is conceivable that the selection or order of the PKD domains integrated onto a material could enable the tuning of the AAV binding and release profiles as well as enhance the capture of a lower affinity serotype, such as AAV4[32] (Figure 1B). Importantly, decorating material surfaces with PKD 1 and PKD 2, which have been recently known as key domains capable of specifically interacting with AAV vectors,[41] can be an alternative method to enhance the specificity of the cys-AAVR system to various AAV serotypes and potentially improve its AAV binding capacity. Further optimization of the cys-AAVR system to facilitate scale-up will, of course, be needed for successful translation toward human application.

Localized/spatially patterned AAV delivery technology can enhance the safety and efficacy for certain applications because off-target localization can elicit immune responses, dilute therapeutic efficacy into irrelevant organs/tissues,[42] or result in transgene toxicity in off-target cells. While decorating the AAV capsid with cell surface receptors/ligands to alter its tissue/organ tropism[42] or regulating transcription by carrying tissue-specific promoters[43,44] has been extensively proposed to limit off-target localization and expression, in general, even after local administration, it is challenging to prevent vector leakage into the circulation, resulting in the systemic spread of AAV capsid antigen and transgene. For example, upon intramuscular injection of AAV9 suspensions, we observed strong gene expression in non-targeted organs such as the heart and liver (Figure 5D). Localized or even spatially patterned gene delivery can better control delivery localization for gene therapy and regenerative medicine applications.[45] Biomaterial systems that can create spatially patterned gene delivery would be beneficial for mimicking spatially organized tissue structures in the body[46] (e.g., aligned tendon and concentric shapes of bone) or stimulating stem cells to induce multi-lineage differentiation within a confined region,[47] particularly for tissue engineering applications. Because PCL and other functionalizable materials can be generated in a broad range of formats and geometries, the system can be further adapted for different modes of delivery and release, ranging from microsphere suspensions and elution from solid three-dimensional polymeric implants to incorporation within hydrogels, for gene therapy and tissue engineering applications.

Capturing AAV vectors without their chemical or genetic modifications followed by injection of the microsphere-adsorbed vector *in vivo* to enable the tissue to "elute" the vector resulted in strong, localized gene expression (Figures 5 and 6). That is, regardless of the viral preparation conditions, simply including the cys-AAVR-biomaterial into vector suspensions can be a highly efficient process to selectively capture AAV and subsequently induce localized gene delivery *in vivo*. This method substantially reduces the number of complex viral preparation steps prior to vector injections, which may be beneficial for increasing the viral yield and reducing product costs.

Conclusions

The cys-AAVR-PCL system is the first to successfully apply the fundamental discovery of AAVR toward novel applications: in this case, the controlled, sustained, and patterned delivery of AAV. The potential of combining viral vectors with engineered biomaterials, which can potentially overcome the limitations associated with current AAV-mediated gene delivery approaches (e.g., off-target gene delivery and the diverse viral binding methods, which differ based on the AAV serotype), was demonstrated in this study. AAVR-displaying

biomaterial systems are thus likely to serve as broad platforms for controlled isolation and delivery of all AAV serotypes, thereby broadening their potential applications from gene therapy to regenerative medicine.

MATERIALS AND METHODS

Production of Cysteine-Modified, Water-Soluble AAVR

Recombinant water-soluble AAVR was expressed in Rosetta(DE3) *E. coli* carrying an expression plasmid (pETDuet-1; Novagen, Madison, WI, USA) that encoded a partial sequence of AAVR (i.e., PKD 1–5), which had been amplified from a KIAA0319L cDNA clone (clone ID 3843301; GE Dharmacon, Lafayette, CO, USA) by using the following primers: 5′- GCTAGGGATCCAGGCGGTGGCGG TAGCTGTTGCTGTGGCGGTGGCGGTAGCGGCGGTGGCGGT AGCGTATCTGCTGGAGAGAGTGTCCAGATAACC-3′ and 5′-GCTAGGCGGCCGCCTACAGGTTGTTTTTCCTGGG-3′. The recombinant AAVR proteins that contained histidine and cysteine tags at the N terminus, which were referred to as cys-AAVR, were extracted from the *E. coli* and harvested by using nickel-charged affinity beads (Ni-nitrilotriacetic acid [NTA]; QIAGEN, Hilden, Germany) according to the manufacturer's guidelines.

Characterization of cys-AAVR

The production of cys-AAVR protein was verified by SDS-PAGE, followed by Coomassie staining (Coomassie Brilliant Blue R-250, BioRad Laboratories, Hercules, CA, USA). The quantity of recombinant cys-AAVR protein was assessed by using a Bicinchoninic Acid Protein (BCA) assay kit (Thermo Fisher Scientific, Waltham, MA, USA). The functionality of cys-AAVR to broadly interact with various AAV serotypes was examined by monitoring the reductions in the transduction efficiencies of AAV vectors after their association with cys-AAVR (0.2 μM). A cell line (HEK293T; 2×10^4) known to be permissive to the majority of wild-type AAV serotypes (i.e., AAV1, -2, -3, -4, -5, -6, -8, and -9 and AAVr3.45) was seeded on 48-well plates 1 day prior to the viral infection. At 48 h post-infection, the percentages of GFP-expressing cells were measured using a flow cytometer at the Yonsei University College of Medicine Medical Research Center (LSR2, BD Bioscience, San Jose, CA, USA).

Fabrication of Polymeric Templates to Anchor cys-AAVR

Biodegradable PCL (80,000 Da, Sigma-Aldrich, St. Louis, MO, USA) polymers were formulated into two different structures: microspheres and nanofibrous matrices. The PCL microspheres were fabricated by using an water-oil single emulsion technique.[34] Briefly, a large-scale process was employed to prepare large numbers of microspheres: 50 mL of 10% (w/v) PCL dissolved in chloroform (Duksan Chemicals, Ansan, Korea) was transferred into 1 L of 2% (w/v) aqueous polyvinylalcohol (PVA, $\overline{M}_n$ = 20,000–30,000 Da; Sigma-Aldrich) solution, and the water-oil phase was emulsified using a homogenizer (HMZ-20N, Poong Lim, Seoul, Korea) for 30 s. The emulsion was magnetically stirred for an additional 2 days to completely evaporate the chloroform (Duksan, Seoul, Korea) from the solidified PCL microspheres; then, these microspheres were settled using a high-speed centrifuge (MEGA 17R, Hanil, Seoul, Korea), vigorously washed five times with distilled water, and filtered through a sieve (diameter = 40 μm; SPL Life Science, Pocheon, Korea) to remove large microspheres. Finally, the PCL microspheres were lyophilized and stored in a desiccator until use. The nanofibrous PCL matrices were fabricated by using an electrospinning technique that has been previously described.[34,48] Briefly, 15% (w/v) PCL dissolved in a mixture (1:1, v/v) of chloroform (Duksan) and dimethylformamide (DMF; Duksan) was electrospun using electrospinning equipment (ESR-100, NanoNC, Seoul, Korea) under 14-kV voltage and using a 15-cm tip-to-collector distance. The flat PCL fibers were collected for 90 min on grounded flat aluminum foil and stored in a desiccator until use.

Surface Modification of PCL Templates with cys-AAVR

The surfaces of the PCL structures were decorated with cys-AAVR proteins via a click-chemistry methodology. Briefly, the PCL structures (i.e., microspheres and electrospun fibers) were immersed in 30% HDA (Sigma-Aldrich) dissolved in isopropanol (Sigma-Aldrich) and gently agitated for 3 h at room temperature to create amines on the PCL surfaces (PCL-NH_2). Subsequently, the aminolyzed PCL surfaces were washed three times with PBS, transferred to Sulfo-SMCC (4 mg/mL; Thermo Fisher Scientific) in PBS solution to create maleimide-displaying PCL surfaces (PCL-click), and kept in a shaking incubator for 1 h. The resulting PCL-click surfaces were rinsed three times with PBS and gently agitated with 0.4 mg/mL cys-AAVR in PBS solution at 4°C overnight. After being washed three times with PBS, the cys-AAVR-conjugated surfaces (cys-AAVR-PCL) were immediately used for anchoring AAV vectors. All the solvents and solutions that were used for conjugating cys-AAVR onto the PCL surfaces were filtered through 0.22 μm syringe filters to assure their sterilization.

Characterization of cys-AAVR-Conjugated PCL Surfaces

The presence of the chemical moieties generated from the series of reactions was verified by Fourier transform infrared (FT-IR) spectroscopy (Spectrum 100, Perkin Elmer, Waltham, MA, USA). The aminolysis of the PCL surfaces was examined by quantifying the number of amines that were displayed on the PCL surfaces by ninhydrin assay, as described elsewhere.[49] Briefly, the aminolyzed surface was immersed in ninhydrin (Sigma-Aldrich) solution (1 M in isopropanol) and incubated at 90°C for 15 min. Once the residual solvent was completely evaporated by cooling the PCL surfaces, 1,4-dioxane (Sigma-Aldrich) was added to dissolve the aminolyzed materials, and isopropanol was included to produce the blue product. The absorbance of the final solution at 560 nm was measured using a spectrophotometer (Nanodrop 2000, Thermo Fisher Scientific) to quantify the presence of amines on the PCL surfaces, and the concentration of the amines was calculated based on a standard curve that was created with serially diluted solutions of HDA. The conjugation of cys-AAVR with the PCL microspheres was visualized by labeling the cys-AAVR with Alexa Fluor 594 (Thermo Fisher Scientific) and imaging the fluorescence using a confocal laser scanning microscope (CLSM; LSM 700, Carl Zeiss, Thornwood, NY, USA). The surface hydrophilicity of the cys-AAVR-PCL systems was examined by

measuring the water contact angles (CAM101, KSV Instruments, Espoo, Finland) on the electrospun fibrous matrices.

Production of AAV Vectors

Eight naturally occurring AAV serotypes, AAV1, -2, 3-, -4, -5, -6, -8, and -9 and an AAV derivative, AAVr3.45, were designed to encode the GFP or luciferase (luc) genes driven by a cytomegalovirus (CMV) promoter and were packaged by a calcium phosphate transient transfection method using an equal amount of three plasmids (17 μg each):[17,50] AAV helper plasmids, which are required for generating each capsid structure (i.e., pXX1, -2, -3, -4, -5, -6, -8, and -9 and pAAVr3.45); plasmids carrying reporter genes (GFP, luc) that are flanked by inverted terminal repeats (ITRs); and an adenoviral helper plasmid (pHelper; Stratagene, La Jolla, CA, USA). These plasmids were electrostatically complexed with calcium cations to transfect AAV293 cells (Stratagene). At 48 h post-transfection, the cells were lysed by a freeze-thawing procedure three times, and the lysed solution that contained the viral vectors was treated with benzonase nuclease (Sigma-Aldrich) to remove fragments of cellular genomes. The resulting AAV vectors were purified by a density gradient method that used iodixanol (OptiPrep, Axis-Shield, Oslo, Norway) and ultracentrifugation (360,000 × *g*; Type 100 Ti rotor, Beckman Coulter, Brea, CA, USA) for 2 h at 18°C. Following these steps, the buffers of each purified viral sample were replaced with 1× PBS-0.01% (v/v) Tween-20 (Sigma-Aldrich) using Amicon tubes (Ultra-15; 10 000 MWCO, Millipore, Billerica, MA, USA) according to the manufacturer's protocol. The genomic DNA of all the viral samples that resisted a deoxyribonuclease (DNase I; Thermo Fisher Scientific) was quantified by qPCR (Mini Opticon, Bio-Rad, Hercules, CA, USA) using SYBR Green master mix (Thermo Fisher Scientific).

In Vitro Characterization of AAV Delivery from cys-AAVR-Conjugated PCL Surfaces

The *in vitro* transduction efficiency of AAV vectors from the cys-AAVR-PCL structures was characterized by measuring the luciferase signal within the transduced cells grown on the PCL electrospun matrices. To examine the deviations of the cellular transduction on the different surfaces, the initial viral quantities on each surface were fixed similarly. The cys-AAVR-PCL electrospun fibers were incubated with AAV2 (1×10^9 vg/matrix) that encoded firefly luciferase (AAV2-luc) for 1 h under gentle shaking. The cellular transduction on the non-modified PCL matrices that contained the adsorbed AAV2 was employed as a control; AAV2 vectors (1×10^9 vg/matrix) were dropped and marginally air-dried on the non-modified PCL matrices without rinsing with PBS to adsorb viral quantities similar to those compared on the cys-AAVR-PCL surfaces. Subsequently, HEK293T cells (1×10^4 cells/matrix) were seeded onto each surface that contained viral vectors. The supernatant in each well was replaced with fresh medium at 3, 6, 9, and 12 days post-culture. At 4, 7, 10, and 13 days post-transduction, the transduced cells on each PCL surface were lysed using a luciferase assay kit (Promega, Madison, WI, USA), and the expression levels of the luciferase that were cumulatively emitted from a cell population were measured using a luminometer (LB96P, EG & G, Berthold, Germany). The results were normalized to the total quantity of the proteins that were expressed from the cells, which was determined using a bicinchoninc acid protein (BCA) assay kit (Thermo Fisher Scientific). The live/dead cells on the cys-AAVR-PCL fibrous matrices were stained by fluorescein diacetate (FDA; Sigma-Aldrich)/propidium iodide (PI; Sigma-Aldrich) and examined using a confocal laser scanning microscope (CLSM; Carl Zeiss) to evaluate the biocompatibility of the cys-AAVR-PCL matrices as a cell culture system. The quantitative analysis on the proliferation of HEK293T cells on the cys-AAVR-PCL matrices was conducted using a CCK-8 (Cell Counting Kit-8; Dojindo Lab, Kumamoto, Japan) assay according to the manufacturer's guidance.

In Vivo Gene Delivery by AAV from cys-AAVR-PCL Microspheres

The localized and sustained AAV delivery from the cys-AAVR-PCL systems was investigated by monitoring the luciferase expression profiles both spatially and temporally in mice following intramuscular injection. Briefly, the cys-AAVR-PCL microspheres (10 mg) were placed in a PBS solution that contained purified AAV9-luc vectors (5×10^{10} vg), and the resulting suspension (10 mg PCL/mouse) was injected into the left hind limb of a mouse (ICR mouse, Orient Bio, Seongnam, Korea) using a syringe (1 mL; Korea Vaccine, Seoul, Korea). At different times after the vector administration, luciferin (10 mg/mL in PBS; 150 μL/g mouse, Promega) was intraperitoneally injected into each mouse, and the time-dependent extent and localization of the luciferase expression were visualized using an IVIS Spectrum imaging system (PerkinElmer, Waltham, MA, USA). Additionally, the muscle tissues were dissected and sectioned using a cryostat microtome (Leica CM 1850, Leica Biosystems, Nussloch, Germany) and stained with H&E (Sigma-Aldrich) to qualitatively analyze the injected tissue. For analyzing the patterned gene delivery using the cys-AAVR-PCL systems, AAV2-luc vectors (3×10^{10} vg) were loaded onto either cys-AAVR-PCL or non-modified PCL electrospun matrices with a V pattern (width × length = 2 × 1 cm); the resulting composites were subcutaneously implanted on the back of mice. The shape of the luciferase signals over the implanted matrices was qualitatively examined at designated time points (6, 10, 20, and 45 days) to determine the time-dependent extent of the patterned gene delivery. Luciferase expression from individual organs was quantified by using a luciferase assay kit (Promega). Briefly, animals were sacrificed 20 days post-injection, and individual organs, including heart, liver, spleen, lung, and muscles, were isolated and processed using a homogenizer (Precellys 24, Bertin Technologies, Villeubanne, France). Subsequently, the homogenized tissues were immersed in lysis buffer (Promega) prior to measuring the luminescence using a luminometer (LB96P). The levels of luminescence (RLU) were normalized to the amount of protein collected from each organ (i.e., RLU/mg protein). *In vivo* inflammatory responses after administrating AAV9 vectors into hindlimb muscle were analyzed by TNF-α in mouse plasma 45 days post-injection. Briefly, blood samples of mice treated with each delivery set were collected at 45 days post-injection and immediately transferred into a K2-EDTA microtube (BD Microtainer, BD Biosciences) to prevent coagulation. After centrifugation, separated plasma was harvested, and 100-fold diluted plasma was analyzed by a TNF-α ELISA kit

(R&D Systems, DY410, Minneapolis, MN, USA) according to the manufacturer's protocols. The quantity of TNF-α was normalized to that of proteins collected from the plasma (pg/mg protein), which was measured using a BCA assay kit (Thermo Fisher Scientific). All of the animal experimental procedures were performed in accordance with the guidelines and under the approval of the Institutional Animal Care and Use Committee of Yonsei University College of Medicine (no. 2016-0092).

Characterization of Viral Release Kinetics from cys-AAVR-PCL Systems

The kinetics of the AAV releases from the cys-AAVR-PCL systems were examined by measuring the fluorescence intensities of Alexa Fluor 594 tagged on the AAV vectors, which were released to the supernatant from cys-AAVR-PCL or non-modified PCL electrospun matrices. Alexa Fluor 594-tagged AAV2 vectors (1×10^9 vg/matrix) were incubated with PCL matrices for 30 min at room temperature and rinsed gently with PBS. To adsorb sufficient viral quantities, AAV2 vectors were marginally air-dried on the non-modified PCL matrices, and their time-dependent release profiles were examined by detecting the fluorescence intensities of Alex Fluor 594, which was tagged onto AAV2 vectors. The supernatant in each well was collected at 0, 1, 3, 12, 24, 48, 96, 168, 240, and 336 h post-incubation and replaced with fresh PBS. The fluorescence intensities of Alexa Fluor 594 were measured using Nanodrop, and the cumulative viral releases were determined as the ratio of the fluorescence intensities measured at designated time points to those quantified at the final time point (i.e., 336 h).

Statistical Analysis

All statistical analyses were performed via one-way ANOVA, followed by Dunnett's post hoc test or Student's t test using SPSS 25.0 software (IBM, New York, NY, USA). All experimental sets were conducted at least in triplicate and are presented as averaged values with SDs.

SUPPLEMENTAL INFORMATION

Supplemental Information can be found online at https://doi.org/10.1016/j.omtn.2019.09.015.

AUTHOR CONTRIBUTIONS

All authors contributed to writing the manuscript. S.K., S.L., H.L., and M.C. conducted the experiments; S.K. and S.L. designed the experiments and wrote the paper; J.H.J. and D.V.S. designed and supervised the experiments; and J.H.J. and D.V.S. wrote the paper. All authors have approved the final version of the manuscript.

CONFLICTS OF INTEREST

The authors declare no competing financial interests.

ACKNOWLEDGMENTS

We would like to thank Dr. Jorge Santiago-Ortiz and Olivia Scheideler for their help in producing the cys-AAVR protein. This research was supported by the Basic Research Lab Program (grant no. 2018025230), Basic Science Research Program (NRF-2018R1A2A2A05020786), and Bio & Medical Technology Development Program (NRF-2017M3A9B4061968, 2018M3A9H2019045, and 2019M3A9H1032791) through the National Research Foundation of Korea (NRF) funded by the Ministry of Science and ICT (MSIT). D.S. was supported by NIH grant R01EY022975. This work was also funded by award 563766 from the Gilbert Family Foundation.

REFERENCES

1. Dismuke, D.J., Tenenbaum, L., and Samulski, R.J. (2013). Biosafety of recombinant adeno-associated virus vectors. Curr. Gene Ther. *13*, 434–452.
2. Kotterman, M.A., and Schaffer, D.V. (2014). Engineering adeno-associated viruses for clinical gene therapy. Nat. Rev. Genet. *15*, 445–451.
3. Asokan, A., Schaffer, D.V., and Samulski, R.J. (2012). The AAV vector toolkit: poised at the clinical crossroads. Mol. Ther. *20*, 699–708.
4. Nathwani, A.C., Reiss, U.M., Tuddenham, E.G., Rosales, C., Chowdary, P., McIntosh, J., Della Peruta, M., Lheriteau, E., Patel, N., Raj, D., et al. (2014). Long-term safety and efficacy of factor IX gene therapy in hemophilia B. N. Engl. J. Med. *371*, 1994–2004.
5. Maguire, A.M., Simonelli, F., Pierce, E.A., Pugh, E.N., Jr., Mingozzi, F., Bennicelli, J., Banfi, S., Marshall, K.A., Testa, F., Surace, E.M., et al. (2008). Safety and efficacy of gene transfer for Leber's congenital amaurosis. N. Engl. J. Med. *358*, 2240–2248.
6. Mendell, J.R., Al-Zaidy, S., Shell, R., Arnold, W.D., Rodino-Klapac, L., Kissel, J.T., Prior, T.W., Miranda, C., Lowes, L., Alfano, L., et al. (2016). Gene therapy for spinal muscular atrophy type 1 shows potential to improve survival and motor functional outcomes. Mol. Ther. *24*, S190–S190.
7. Carpentier, A.C., Frisch, F., Labbé, S.M., Gagnon, R., de Wal, J., Greentree, S., Petry, H., Twisk, J., Brisson, D., and Gaudet, D. (2012). Effect of alipogene tiparvovec (AAV1-LPL(S447X)) on postprandial chylomicron metabolism in lipoprotein lipase-deficient patients. J. Clin. Endocrinol. Metab. *97*, 1635–1644.
8. Wang, L., Wang, H., Bell, P., McCarter, R.J., He, J., Calcedo, R., Vandenberghe, L.H., Morizono, H., Batshaw, M.L., and Wilson, J.M. (2010). Systematic evaluation of AAV vectors for liver directed gene transfer in murine models. Mol. Ther. *18*, 118–125.
9. Orkin, S.H., and Reilly, P. (2016). MEDICINE. Paying for future success in gene therapy. Science *352*, 1059–1061.
10. Jang, J.H., Schaffer, D.V., and Shea, L.D. (2011). Engineering biomaterial systems to enhance viral vector gene delivery. Mol. Ther. *19*, 1407–1415.
11. Madrigal, J.L., Stilhano, R., and Silva, E.A. (2017). Biomaterial-guided gene delivery for musculoskeletal tissue repair. Tissue Eng. Part B Rev. *23*, 347–361.
12. Jang, J.H., and Shea, L.D. (2006). Intramuscular delivery of DNA releasing microspheres: microsphere properties and transgene expression. J. Control. Release *112*, 120–128.
13. Mah, C., Fraites, T.J., Jr., Zolotukhin, I., Song, S., Flotte, T.R., Dobson, J., Batich, C., and Byrne, B.J. (2002). Improved method of recombinant AAV2 delivery for systemic targeted gene therapy. Mol. Ther. *6*, 106–112.
14. McConnell, K.I., Gomez, E.J., and Suh, J. (2012). The identity of the cell adhesive protein substrate affects the efficiency of adeno-associated virus reverse transduction. Acta Biomater. *8*, 4073–4079.
15. Kim, E., Lee, S., Hong, S., Jin, G., Kim, M., Park, K.I., Lee, H., and Jang, J.H. (2014). Sticky "delivering-from" strategies using viral vectors for efficient human neural stem cell infection by bioinspired catecholamines. ACS Appl. Mater. Interfaces *6*, 8288–8294.
16. Kim, J.S., Chu, H.S., Park, K.I., Won, J.I., and Jang, J.H. (2012). Elastin-like polypeptide matrices for enhancing adeno-associated virus-mediated gene delivery to human neural stem cells. Gene Ther. *19*, 329–337.
17. Lee, S., Kim, J.S., Chu, H.S., Kim, G.W., Won, J.I., and Jang, J.H. (2011). Electrospun nanofibrous scaffolds for controlled release of adeno-associated viral vectors. Acta Biomater. *7*, 3868–3876.

18. Lee, H.H., Haleem, A.M., Yao, V., Li, J., Xiao, X., and Chu, C.R. (2011). Release of bioactive adeno-associated virus from fibrin scaffolds: effects of fibrin glue concentrations. Tissue Eng. Part A *17*, 1969–1978.

19. Dupont, K.M., Boerckel, J.D., Stevens, H.Y., Diab, T., Kolambkar, Y.M., Takahata, M., Schwarz, E.M., and Guldberg, R.E. (2012). Synthetic scaffold coating with adeno-associated virus encoding BMP2 to promote endogenous bone repair. Cell Tissue Res. *347*, 575–588.

20. Jang, J.H., Koerber, J.T., Gujraty, K., Bethi, S.R., Kane, R.S., and Schaffer, D.V. (2010). Surface immobilization of hexa-histidine-tagged adeno-associated viral vectors for localized gene delivery. Gene Ther. *17*, 1384–1389.

21. Li, H., Zhang, F.L., Shi, W.J., Bai, X.J., Jia, S.Q., Zhang, C.G., and Ding, W. (2015). Immobilization of FLAG-tagged recombinant adeno-associated virus 2 onto tissue engineering scaffolds for the improvement of transgene delivery in cell transplants. PLoS ONE *10*, e0129013.

22. Summerford, C., and Samulski, R.J. (1998). Membrane-associated heparan sulfate proteoglycan is a receptor for adeno-associated virus type 2 virions. J. Virol. *72*, 1438–1445.

23. Walters, R.W., Yi, S.M., Keshavjee, S., Brown, K.E., Welsh, M.J., Chiorini, J.A., and Zabner, J. (2001). Binding of adeno-associated virus type 5 to 2,3-linked sialic acid is required for gene transfer. J. Biol. Chem. *276*, 20610–20616.

24. Burova, E., and Ioffe, E. (2005). Chromatographic purification of recombinant adenoviral and adeno-associated viral vectors: methods and implications. Gene Ther. *12* (*Suppl 1*), S5–S17.

25. Pillay, S., Meyer, N.L., Puschnik, A.S., Davulcu, O., Diep, J., Ishikawa, Y., Jae, L.T., Wosen, J.E., Nagamine, C.M., Chapman, M.S., and Carette, J.E. (2016). An essential receptor for adeno-associated virus infection. Nature *530*, 108–112.

26. Hoyle, C.E., and Bowman, C.N. (2010). Thiol-ene click chemistry. Angew. Chem. Int. Ed. Engl. *49*, 1540–1573.

27. Jang, J.H., Koerber, J.T., Kim, J.S., Asuri, P., Vazin, T., Bartel, M., Keung, A., Kwon, I., Park, K.I., and Schaffer, D.V. (2011). An evolved adeno-associated viral variant enhances gene delivery and gene targeting in neural stem cells. Mol. Ther. *19*, 667–675.

28. Hwang, J.H., Lee, S., Kim, E., Kim, J.S., Lee, C.H., Ahn, I.S., and Jang, J.H. (2011). Heparin-coated superparamagnetic nanoparticle-mediated adeno-associated virus delivery for enhancing cellular transduction. Int. J. Pharm. *421*, 397–404.

29. Kotterman, M.A., Vazin, T., and Schaffer, D.V. (2015). Enhanced selective gene delivery to neural stem cells in vivo by an adeno-associated viral variant. Development *142*, 1885–1892.

30. Kim, Y., Kim, E., Oh, S., Yoon, Y.E., and Jang, J.H. (2018). Mutagenic Analysis of an Adeno-Associated Virus Variant Capable of Simultaneously Promoting Immune Resistance and Robust Gene Delivery. Hum. Gene Ther. *29*, 25–41.

31. Cho, M., Jung, K., Kim, S.H., Kim, I.S., Kim, M., Shin, M., Lee, H., Park, K.I., and Jang, J.H. (2019). Safety and efficacy evaluations of an adeno-associated virus variant for preparing IL10-secreting human neural stem cell-based therapeutics. Gene Ther. *26*, 135–150.

32. Dudek, A.M., Pillay, S., Puschnik, A.S., Nagamine, C.M., Cheng, F., Qiu, J., Carette, J.E., and Vandenberghe, L.H. (2018). An Alternate Route for Adeno-associated Virus (AAV) Entry Independent of AAV Receptor. J. Virol. *92*, e012213–e012217.

33. Varde, N.K., and Pack, D.W. (2004). Microspheres for controlled release drug delivery. Expert Opin. Biol. Ther. *4*, 35–51.

34. Kim, M., Kim, J.S., Lee, H., and Jang, J.H. (2016). Polydopamine-decorated sticky, water-friendly, biodegradable polycaprolactone cell carriers. Macromol. Biosci. *16*, 738–747.

35. Jgamadze, D., Bergen, J., Stone, D., Jang, J.H., Schaffer, D.V., Isacoff, E.Y., and Pautot, S. (2012). Colloids as mobile substrates for the implantation and integration of differentiated neurons into the mammalian brain. PLoS ONE *7*, e30293.

36. Lee, S., Jin, G., and Jang, J.H. (2014). Electrospun nanofibers as versatile interfaces for efficient gene delivery. J. Biol. Eng. *8*, 30.

37. Jin, G., Shin, M., Kim, S.H., Lee, H., and Jang, J.H. (2015). SpONGE: spontaneous organization of numerous-layer generation by electrospray. Angew. Chem. Int. Ed. Engl. *54*, 7587–7591.

38. Lee, S., Yun, S., Park, K.I., and Jang, J.H. (2016). Sliding fibers: slidable, injectable, and gel-like electrospun nanofibers as versatile cell carriers. ACS Nano *10*, 3282–3294.

39. Tarantal, A.F., Lee, C.C.I., Martinez, M.L., Asokan, A., and Samulski, R.J. (2017). Systemic and persistent muscle gene expression in rhesus monkeys with a liver de-targeted adeno-associated virus vector. Hum. Gene Ther. *28*, 385–391.

40. Pillay, S., Zou, W., Cheng, F., Puschnik, A.S., Meyer, N.L., Ganaie, S.S., Deng, X., Wosen, J.E., Davulcu, O., Yan, Z., et al. (2017). Adeno-associated Virus (AAV) Serotypes Have Distinctive Interactions with Domains of the Cellular AAV Receptor. J. Virol. *91*, e00391–e00317.

41. Zhang, R., Cao, L., Cui, M., Sun, Z., Hu, M., Zhang, R., Stuart, W., Zhao, X., Yang, Z., Li, X., et al. (2019). Adeno-associated virus 2 bound to its cellular receptor AAVR. Nat. Microbiol. *4*, 675–682.

42. Waehler, R., Russell, S.J., and Curiel, D.T. (2007). Engineering targeted viral vectors for gene therapy. Nat. Rev. Genet. *8*, 573–587.

43. Toscano, M.G., Romero, Z., Muñoz, P., Cobo, M., Benabdellah, K., and Martin, F. (2011). Physiological and tissue-specific vectors for treatment of inherited diseases. Gene Ther. *18*, 117–127.

44. Falk, D.J., Mah, C.S., Soustek, M.S., Lee, K.Z., Elmallah, M.K., Cloutier, D.A., Fuller, D.D., and Byrne, B.J. (2013). Intrapleural administration of AAV9 improves neural and cardiorespiratory function in Pompe disease. Mol. Ther. *21*, 1661–1667.

45. Park, J., Decker, J.T., Margul, D.J., Smith, D.R., Cummings, B.J., Anderson, A.J., and Shea, L.D. (2018). Local Immunomodulation with Anti-inflammatory Cytokine-Encoding Lentivirus Enhances Functional Recovery after Spinal Cord Injury. Mol. Ther. *26*, 1756–1770.

46. Pawar, K., Cummings, B.J., Thomas, A., Shea, L.D., Levine, A., Pfaff, S., and Anderson, A.J. (2015). Biomaterial bridges enable regeneration and re-entry of corticospinal tract axons into the caudal spinal cord after SCI: Association with recovery of forelimb function. Biomaterials *65*, 1–12.

47. Adil, M.M., Rodrigues, G.M.C., Kulkarni, R.U., Rao, A.T., Chernavsky, N.E., Miller, E.W., and Schaffer, D.V. (2017). Efficient generation of hPSC-derived midbrain dopaminergic neurons in a fully defined, scalable, 3D biomaterial platform. Sci. Rep. *7*, 40573.

48. Cho, M., Kim, S.H., Jin, G., Park, K.I., and Jang, J.H. (2016). Salt-induced electrospun patterned bundled fibers for spatially regulating cellular responses. ACS Appl. Mater. Interfaces *8*, 13320–13331.

49. Gümüşderelioğlu, M., Dalkıranoğlu, S., Aydın, R.S., and Cakmak, S. (2011). A novel dermal substitute based on biofunctionalized electrospun PCL nanofibrous matrix. J. Biomed. Mater. Res. A *98*, 461–472.

50. Asuri, P., Bartel, M.A., Vazin, T., Jang, J.H., Wong, T.B., and Schaffer, D.V. (2012). Directed evolution of adeno-associated virus for enhanced gene delivery and gene targeting in human pluripotent stem cells. Mol. Ther. *20*, 329–338.